Final Draft
of the original manuscript:

Graff, S.; Steglich, D.; Brocks, W.:
Forming of Magnesium - Crystal Plasticity and Plastic Potentials
In: Advanced Engineering Materials (2007) Wiley

DOI: 10.1002/adem.200700162

Forming of Magnesium - Crystal Plasticity and Plastic Potentials

Stéphane Graff, Dirk Steglich, Wolfgang Brocks

GKSS Research Centre,
Institute for Materials Research, Mechanics of Materials,
Geesthacht, Germany

dirk.steglich@gkss.de

Abstract.

Magnesium alloys show a deformation behaviour, which is quite different from that of other lightweight materials like aluminium. What constitutes the difference is the respective crystalline structure, namely hexagonal close-packed (hcp) for magnesium and face-centred cubic (fcc) for aluminium. Capturing the special features of the deformation phenomena of magnesium hence requires accounting for the microstructural mechanisms. This is realised with the help of crystal plasticity. The specific slip mechanisms occurring in magnesium are identified and single crystals as well as textured polycrystals are analysed numerically. Comparing with results of channel-die tests yields the parameters of the model. Finally, yield surfaces are generated by virtual testing of representative volume elements and a phenomenological anisotropic yield function is established. The linking of micro- and mesoscale provides a procedure for the simulation of the yielding and hardening behaviour of arbitrarily textured solids with hcp structure.

Keywords: hcp metals, magnesium, crystal plasticity, twinning, yield surface, anisotropy, forming.

1 Introduction

The low density of magnesium (1.74 g/cm^3) and its relatively high specific strength constitute its attractiveness for applications in transportation industries, where saving of structural weight and reduction of fuel consumption are urgent challenges. The still moderate formability of magnesium alloys obstructs a broad application, however. Developing alloys with improved properties demands a deeper understanding of the controlling deformation mechanisms, first of all, and reli-

able simulation tools for predicting the forming capabilities in the next step. Last but not least, the structural behaviour under mechanical loads and the lifetime of the component has to be assessed. Conventional constitutive models of plasticity fail if applied to magnesium. Adequate models have to account for several anomalies of the mechanical behaviour. Magnesium and its alloys show a pronounced strength differential effect at low homologous temperatures, i.e. the tensile strength is much higher than the strength in compression. Furthermore, magnesium exhibits a low ductility as well as strong deformation anisotropy.

These anomalies in the mechanical behaviour of magnesium originate from its hexagonal close-packed (hcp) crystallographic structure. Hcp metals hold a reduced number of available slip systems compared to body-centred cubic (bcc) and face-centred cubic (fcc) lattices, making plastic deformation more difficult. With the asymmetric distribution of slip systems over the crystallographic reference sphere, various primary and secondary slip and twinning mechanisms can and have to be activated at the same time. Understanding the mechanisms of dislocation gliding and deformation twinning for single crystals and polycrystalline aggregates constitutes the foundation for modelling of the macroscopic mechanical behaviour. To this end, microstructural experimental observations, mechanical tests and numerical modelling are combined.

Channel-die compression tests on Mg single crystals for various crystallographic orientations and on textured and polycrystals have been conducted by Kelley and Hosford [1,2]. Their data are used to identify the parameters of a crystal plasticity model. The model is then applied for predicting the mesoscopic deformation of polycrystalline representative volume elements (RVEs). In this way the microscopic features developing during plastic deformation of Mg are linked to the mesoscale and allow for predicting the yielding behaviour of arbitrarily textured solids, for example rolled plates.

Due to limitations in computational power, simulations of the behaviour of macroscopic structures cannot be performed effectively based on models of crystal plasticity. They require constitutive equations to be used in the framework of phenomenological plasticity, i.e. a plastic potential and a flow rule. The presented method can be used to calibrate parameters of any plastic potential. Here, the plastic potential proposed by Cazacu and Barlat [3] is used for the simulation of a cup-forming process.

2 Deformation mechanisms and test configuration

The deformation mechanism in magnesium in relation to its crystallographic planes have been studied intensively over the years, starting with investigations by Hauser et al.[4], Reed-Hill and Robertson[5], Yoshinaga and Horiuchi[6]. Any somewhat complete reference list would exceed the limitations of the present report. Modelling activities started recently and concentrate on the alloy AZ31 as the most common wrought magnesium alloy, see e.g. Agnew et al.[7,8], Staroselsky and Anand[9]. Resuming the results, the relevant deformation mechanisms of magnesium and its alloys are still subjected to discussion. Generally, any prismatic $\langle \mathbf{a} \rangle$ and one pyramidal $\langle \mathbf{a}+\mathbf{c} \rangle$ slip system family additionally to basal slip and tensile twinning appear to be necessary for a com-

plete description. Since pyramidal $\langle \mathbf{a} \rangle$ slip is equivalent to a combination of basal and prismatic $\langle \mathbf{a} \rangle$ cross-slip, this particular system will not be considered in the following calculations. The primary systems basal $\langle \mathbf{a} \rangle$, prismatic $\langle \mathbf{a} \rangle$, pyramidal $\langle \mathbf{a}+\mathbf{c} \rangle$ slip plus tensile twinning on $\{10\bar{1}2\}$ are chosen here to model the mechanical behaviour in the framework of crystal plasticity. These families include three basal, three prismatic, six pyramidal and six twinning systems. Table 1 summarizes the considered deformation modes.

Name	# of Slip Systems	Plane	Slip Direction
Basal $\langle \mathbf{a} \rangle$	3	$\{0001\}$	$\langle 11\bar{2}0 \rangle$
Prismatic $\langle \mathbf{a} \rangle$	3	$\{\bar{1}100\}$	$\langle 11\bar{2}0 \rangle$
Pyramidal $\langle \mathbf{a}+\mathbf{c} \rangle$	6	$\{11\bar{2}2\}$	$\langle 11\bar{2}3 \rangle$
Tensile Twin	6	$\{10\bar{1}2\}$	$\langle 10\bar{1}1 \rangle$

Table 1: Deformation modes considered

The kinematical theory for the mechanics of crystals has been established in the pioneering work of Taylor[10] and the theory by Hill[11], Rice[12], Hill and Rice[13]. The model of crystal plasticity used here employs the framework of Peirce et al.[14] and Asaro[15,16]. The implementation in the commercial finite element code ABAQUS is based on the user-material routine of Huang[17]. The theoretical background is shortly outlined in the following. The complete set of equations used to describe the deformation behaviour of each slip system is described by Graff[17].

The crystalline material undergoes elastic stretching, rotation and plastic deformation. where the latter is assumed to arise solely from crystalline slip. The total deformation gradient, **F**, is decomposed in two parts, one describing plastic shear of the material, $\mathbf{F}^{\mathrm{p}}$, and the second stretching and rotation of the lattice. The rate of change of $\mathbf{F}^{\mathrm{p}}$ is related to the slip rate $\dot{\gamma}^{(\alpha)}$ of the α slip system by

$$\dot{\mathbf{F}}^{\mathrm{p}} \cdot \mathbf{F}^{\mathrm{p}-1} = \sum_{\alpha} \dot{\gamma}^{(\alpha)} \mathbf{m}^{(\alpha)} \mathbf{n}^{(\alpha)}, \tag{1}$$

where the sum ranges over all activated slips systems, and the unit vectors $\mathbf{m}^{(\alpha)}$, $\mathbf{n}^{(\alpha)}$ are the slip direction and the slip-plane normal, respectively. The crystalline slip is assumed to obey Schmid's law, i.e. the slipping rate $\dot{\gamma}^{(\alpha)}$ depends on Cauchy's stress tensor, **T**, solely through Schmid's resolved shear stresses,

$$\tau^{(\alpha)} = \mathbf{n}^{*(\alpha)} \cdot \frac{\rho_0}{\rho} \mathbf{T} \cdot \mathbf{m}^{*(\alpha)}, \tag{2}$$

where ρ_0 and ρ are the mass densities in the reference and current states. According to Peirce et al.[14], the constitutive equation of slip is assumed as a viscoplastic power law,

$$\frac{\dot{\gamma}^{(\alpha)}}{\dot{\gamma}_0^{(\alpha)}} = \left| \frac{\tau^{(\alpha)}}{\tau_{\mathrm{Y}}^{(\alpha)}} \right|^n \operatorname{sign}\left(\frac{\tau^{(\alpha)}}{\tau_{\mathrm{Y}}^{(\alpha)}} \right), \tag{3}$$

where $\dot{\gamma}_0^{(\alpha)}$ is a reference strain rate, $\tau_Y^{(\alpha)}$ characterises the current strength of the α slip system, and n is the rate sensitivity exponent. Strain hardening is characterized by the evolution of the strengths

$$\dot{\tau}_Y^{(\alpha)} = \sum_\beta h_{\alpha\beta}\left(\bar{\gamma}\right)\dot{\gamma}^{(\alpha)} \,, \tag{4}$$

with $h_{\alpha\beta}$ being the self ($\alpha = \beta$) and latent ($\alpha \neq \beta$) hardening moduli depending on Taylor's cumulative shear strain on all slip systems,

$$\bar{\gamma} = \sum_\alpha \int_0^t \left|\dot{\gamma}^{(\alpha)}\right| d\tau \,. \tag{5}$$

According to Table 1, the slip systems are grouped into four families where twinning is treated like slip.

In order to study the deformation mechanisms of pure magnesium, Kelley and Hosford[1,2] performed channel-die compression tests as shown in Figure 1 on single crystals and on textured magnesium samples cut out of a rolled plate. Small cuboids of approximately 6×10×13 mm^3 were compressed in a steel channel in one direction, while deformation in the second direction was constrained and the third one was free. By changing the initial orientation of the samples, see Table 2 for the single crystals, different slip and slip/twinning modes can be activated. The experimental results of Kelley and Hosford are used here as a reference, from which critical resolved shear stresses for each of the slip systems as well as hardening parameters have been calibrated.

test	loading (1)	constraint (2)
A	$\langle 0\,0\,0\,1\rangle$	$\langle 1\,0\,\bar{1}\,0\rangle$
B	$\langle 0\,0\,0\,1\rangle$	$\langle 1\,\bar{2}\,1\,0\rangle$
C	$\langle 1\,0\,\bar{1}\,0\rangle$	$\langle 0\,0\,0\,1\rangle$
D	$\langle 1\,\bar{2}\,1\,0\rangle$	$\langle 0\,0\,0\,1\rangle$
E	$\langle 1\,0\,\bar{1}\,0\rangle$	$\langle 1\,\bar{2}\,1\,0\rangle$
F	$\langle 1\,\bar{2}\,1\,0\rangle$	$\langle 1\,0\,\bar{1}\,0\rangle$
G	$\langle 0\,0\,0\,1\rangle$ at 45°	$\langle 1\,0\,\bar{1}\,0\rangle$

Table 2: Definition of the different orientations used with the channel-die compression tests on single crystals by Kelley and Hosford[1,2]

The die and the loading punch are modelled as rigid surfaces. Friction between the sample and the rigid surfaces is accounted for, assuming a Coulomb friction coefficient of 0.05 for all tests. Since the experiments have been performed with quasistatic loading, a strain rate sensitivity exponent n = 50 is taken in Equation (3), making the simulation results almost rate independent. The reference strain rate of $\dot{\gamma}_0^{(\alpha)} = 10^{-3}$ is chosen for all slip systems to be compatible with the

time scale in the FE simulations.

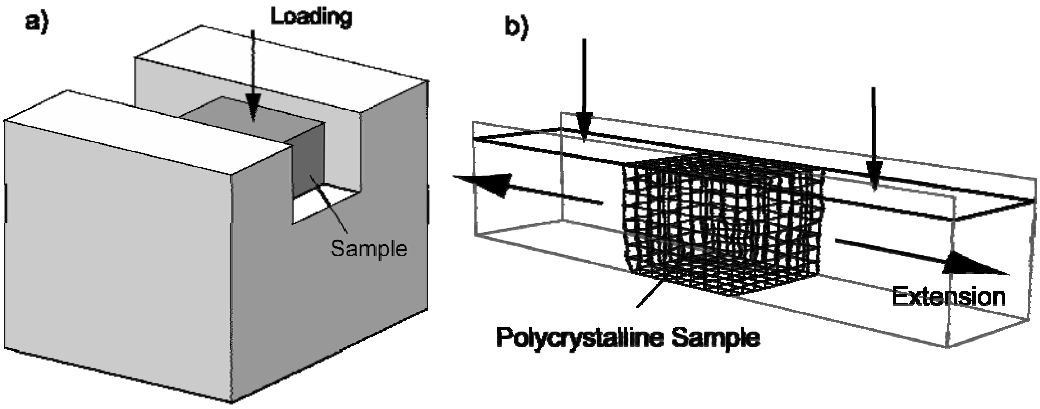

Fig. 1: Channel-die compression test: (a) schematic view and (b) FE model of a polycrystal

A comparison of simulation and test results for single crystals of orientations **A** to **G**, see Table 2, is shown in Fig. 2. A good qualitative and quantitative agreement between experimental and simulated results is obtained. Particularly, the simulations capture the anomalous hardening behaviour of orientations **E** and **F** with relatively low yield stress and almost no hardening at strains smaller than 6%, followed by a sudden increase in stress, which is typical for activation and saturation of deformation twinning.

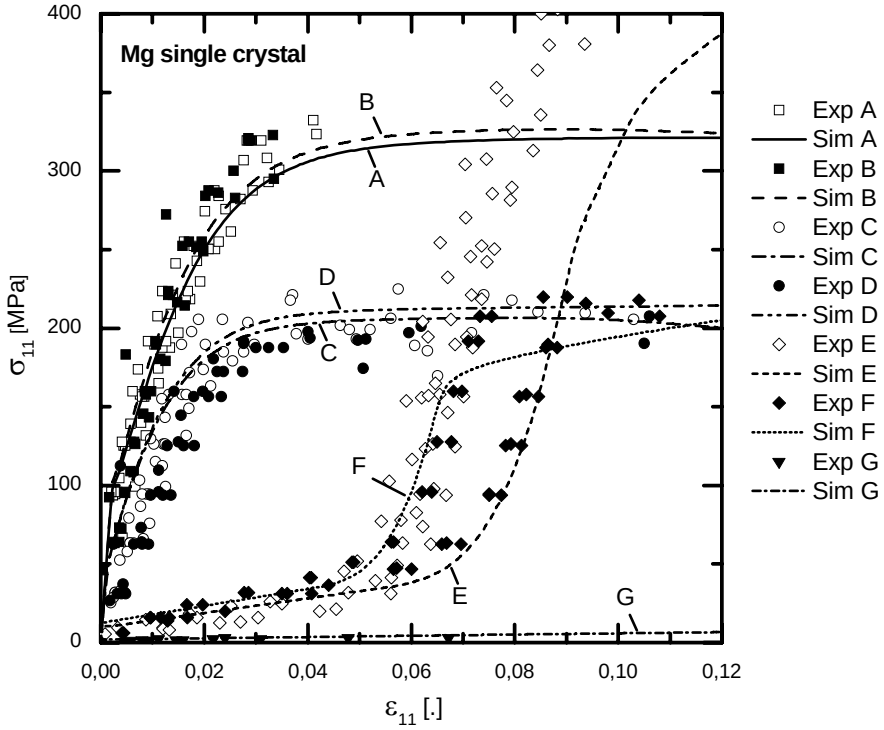

Fig. 2: Channel-die compression tests of pure Mg single crystal: simulation results and tests (Kelly and Hosford, 1968a).

Fig. 3 displays the respective results for the polycrystalline samples cut from a textured rolled plate. The orientations with respect to compression loading and applied constraint for the polycrystalline case are indicated by two of the letters L (longitudinal or rolling), T (transverse) and S (short transverse or thickness), where the first letter denotes the loading direction and the second the constraint direction. The simulations of compression tests in L, T and S-direction were performed on polycrystalline aggregates of 8×8×8 solid elements.

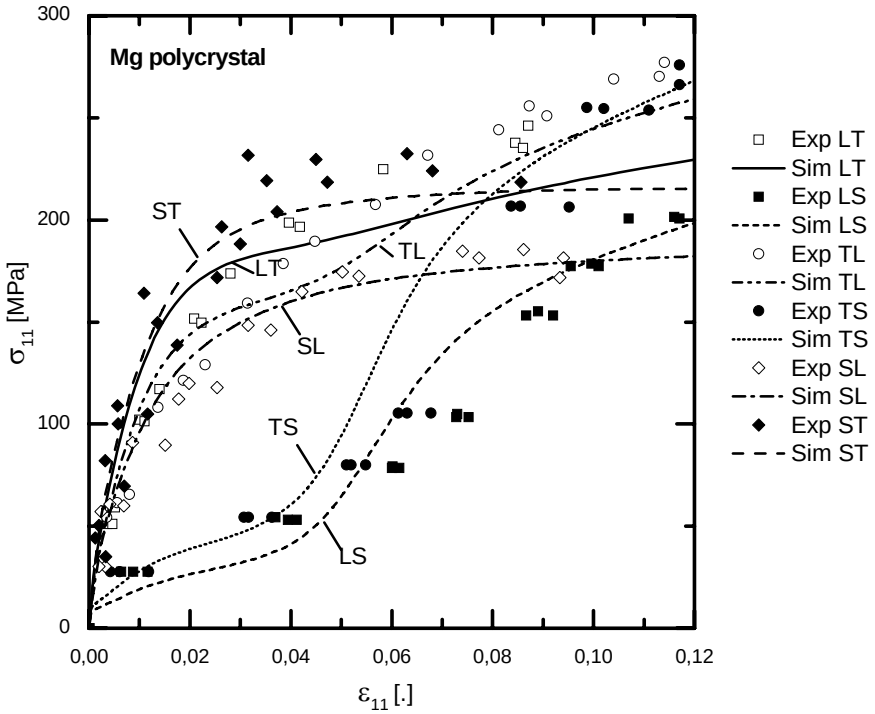

Fig. 3: Channel-die compression tests of textured Mg rolled plate material, simulation and test results (Kelly and Hosford[1,2])

3 Yield Surfaces of Polycrystals

As simulations of the structural behaviour of polycrystals can hardly be performed with crystal plasticity models formulated on the micro-scale, the next step in the modelling chain is the prediction of yield loci and strain hardening in the (L,T)-plane of the rolled material and the fitting of these numerically generated isocontours by an analytical expression of the yield potential. To this end, the same polycrystalline aggregate is investigated under biaxial loading conditions performing radial in-plane loading paths with different ratios of $\sigma_T/\sigma_L = \arctan\varphi$, where φ is the angle to the rolling direction (L) of the plate. For each loading path, several unloading steps have been realised in order to separate elastic and plastic mesoscopic strain. Periodic boundary conditions were applied on the surfaces of the RVE. The results are depicted in Fig. 4 a and 4 b as dashed lines with symbols.

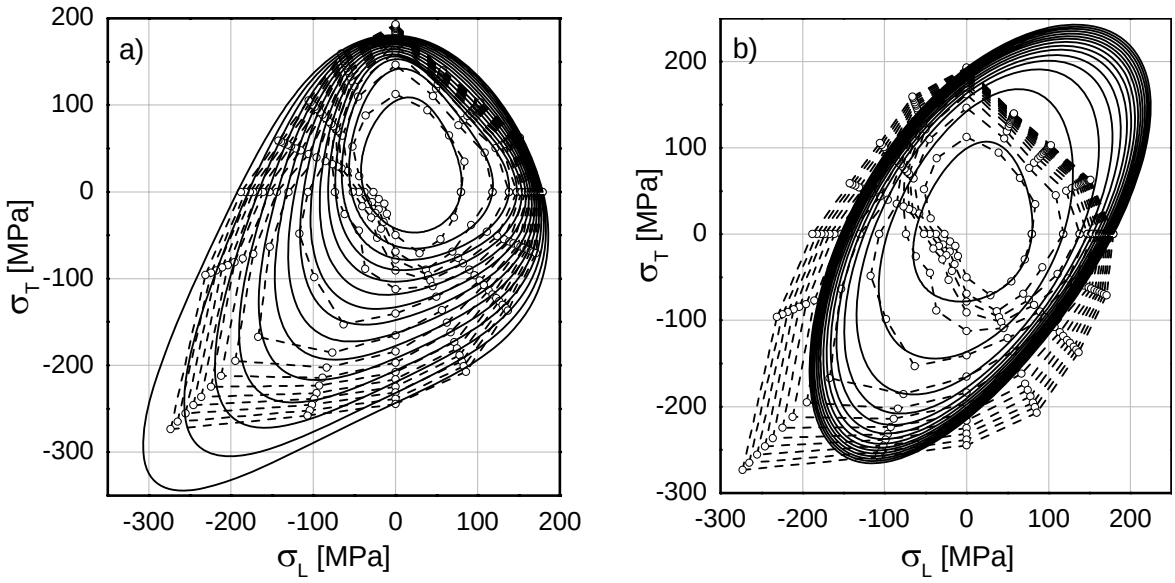

Fig. 4: Yield surfaces and hardening obtained from biaxially loaded RVEs (dashed lines with symbols) in comparison with predictions of the Cazacu & Barlat model: parameter fit using a quadratic function (a) and an exponential function (b) of equivalent plastic strain

A phenomenological yield potential for textured magnesium has to account for both anisotropy and the asymmetry under tension or compression, which is due to the activation of twinning. Accounting for latter, namely shifting the centre of the yield surface out of the origin of the deviatoric plane, requires including the third invariant of the stress tensor. Cazacu and Barlat (2004) have proposed the following yield potential

$$f^0 \equiv \left(J_2^0\right)^{\frac{3}{2}} - cJ_3^0 = \tau_Y^3 . \tag{6}$$

where J_2^0 and J_3^0 are generalisations of the second and third invariant of the stress tensor for orthotropic materials, containing 6 and 11 model parameters, respectively, in the general three-dimensional case. The total number of model parameters reduces to 7 in the plane stress case. Different from the yield criteria of von Mises and Hill, convexity of the yield surface is not a priori ensured and has therefore to be introduced as an additional side condition, while identifying the respective parameters, in order to meet Drucker's postulate of material stability.

In order to describe the strain hardening of the material, the parameters J_2^0 and J_3^0 have been taken to be dependent on the equivalent plastic strain. Two types of functions have been assumed to describe this dependency: quadratic functions and saturating exponential laws. The fitting process has been carried out using a least-square fit minimising the difference between Equation (6) and the yield contours predicted by the polycrystalline RVE. The results are also displayed in Figure 4 as solid lines. With the quadratic dependence (Fig. 4a), a good agreement between the mesoscale and the phenomenological yield surfaces, whereas for the exponential one (Fig. 4b), the fit is less satisfying as the hardening in tension is not well reproduced by the phenomenologi-

cal model. However, considering the ratio of transverse and short transverse strain, i.e. the so-called Lankford coefficient, *r*, the exponential fit yields a more realistic approximation, which matches the order of magnitude, at least.

The *r*-value has a strong effect on the shape and the quality of formed products. As an example, the forming analysis of a cylindrical cup leads to different predictions of the cup's shape. Low values of *r* as obtained by the quadratic hardening functions will cause a thickness reduction of the sheet and the "earing" due to anisotropic deformation is less pronounced. Higher *r*-values will cause deformation mainly in the sheet plane, consequently the "earing" is more pronounced (see exp-fit in Figure 5b).

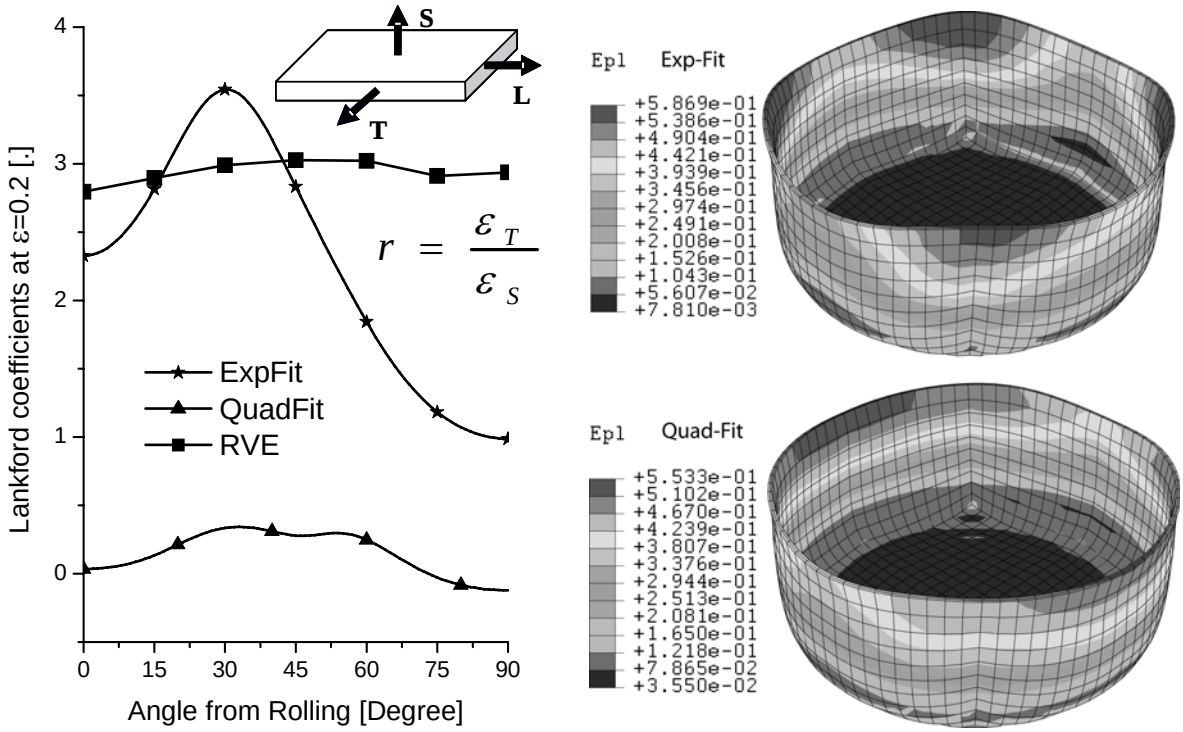

Fig. 5: Lankford coefficients (*r*-values) resulting from two different parameter fits: the different yield loci (a) and predictions of the plastic equivalent strain in cup forming using the two fits from Fig. 4(b)

4 Conclusions

A crystal plasticity model has been used to study the deformation mechanisms of magnesium. Simulations of channel-die compression tests and uniaxial tension and compression tests revealed that the anomalous deformation behaviour can be understood considering four deformation mechanisms and their activation. Once the material parameters of crystal plasticity have been identified, they can be used for predicting the mechanical response of arbitrarily textured polycrystalline materials by building aggregates of single crystals. For application to the analysis of structural components, a phenomenological yield potential and a respective hardening rule has been established. A satisfactory formulation of hardening of magnesium is still an open question, however. The presented methodology links investigations on the micro-level with simulation

techniques used on the length scale of engineering structures.

5 Acknowledgement

The authors acknowledge W. Hosford's support while providing the primary data of his pioneering experimental work on pure magnesium.

6 References

[1] E.W. Kelley, W.F. Hosford, *Trans. Metall. Soc. AIME* **1968**, 242, 5.

[2] E.W. Kelley, W.F. Hosford, *Trans. Metall. Soc. AIME,* **1968**, 242, 654.

[3] O. Cazacu, F. Barlat, *Int. J. Plasticity,* **2004**, 20, 2027.

[4] F.E. Hauser, P.R. Landon, J.E. Dorn, *Trans. ASM*, **1956**, 48, 986.

[5] R.E. Reed-Hill, W.E. Robertson, *Trans. Metall. Soc. AIME*, **1957**, 209. 496.

[6] H. Yoshinaga, R. Horiuchi, *Trans. Jpn. I. JIM*, **1963**, 5, 14.

[7] S.R. Agnew, M.H. Yoo, C.N. Tomé, *Acta Mater*., **2001**, 49, 4277.

[8] S.R. Agnew, C.N. Tomé, D.W. Brown, T.M. Holden, S.C. Vogel, *Scripta Mater*., **2003**, 48, 1003.

[9] A. Staroselsky, L. Anand, *Int. J. Plasticity*, **2003**, 19, 1843.

[10] G.I. Taylor, *J. I. Met*., **1938**, 62, 307.

[11] R. Hill, *J. Mech. Phys. Solids*, **1966**, 15, 95.

[12] J.R. Rice, *J. Mech. Phys. Solids*, **1971**, 19, 433.

[13] R. Hill, J.R. Rice, *J. Mech. Phys. Solids*, **1972**, 20, 401.

[14] D. Peirce, R.J. Asaro, A. Needleman, *Acta Metall*., **1983**, 31, 1951.

[15] R.J. Asaro, *J. Appl. Mech*., **1983**, 50, 921.

[16] R.J. Asaro, *Adv. Appl. Mech*., **1983**, 23, 1.

[17] Y. Huang, Report MECH-178, Div. Applied Science, Harvard University, Cambridge (MA), **1991**.

[18] S. Graff, PhD Thesis, TU Berlin, **2007**.